JOURNAL OF GUIDANCE, CONTROL, AND DYNAMICS
Vol. 22, No. 2, March–April 1999

Autonomous Orbit Determination for Two Spacecraft from Relative Position Measurements

Mark L. Psiaki*
Cornell University, Ithaca, New York 14853-7501

A batch filter has been designed and analyzed to autonomously determine the orbits of two spacecraft based on measurements of the relative position vector from one spacecraft to the other. This system provides a means for high-precision autonomous orbit determination for systems that cannot be dependent on signals from the global positioning system constellation or ground stations. The filter uses a time series of the inertially referenced relative position vector, and it uses orbital dynamics models for the two spacecraft. It estimates the 6-element orbital state vectors of both spacecraft along with a drag parameter for each one. The observability of this system is demonstrated in this proof-of-concept study, and the filter's best-case achievable position accuracy is estimated for a number of situations. Position accuracies on the order of 1-m rms may be possible for certain configurations.

I. Introduction

KNOWLEDGE of orbit and position is a practical requirement for all Earth-orbiting spacecraft. Traditional methods of orbit determination rely on ground-based tracking measurements of range and range rate.[1] Newer techniques use signals from global positioning system (GPS) receivers.[2,3] Autonomous methods are based solely on data from sensors that are onboard the spacecraft. Several types of autonomous systems have been proposed or developed.[4–7]

Some satellite systems have an autonomous orbit determination requirement that stems from military considerations. In the event of a war, ground-based or GPS-based orbit determination aids may be destroyed, or their signals may be jammed. Therefore, there is a need for autonomous orbit determination capabilities beyond those that can be provided by an onboard GPS receiver.

This paper analyzes an idea for autonomous orbit determination of Earth-orbiting spacecraft that was first proposed and analyzed by Markley.[7] The basic idea is to simultaneously determine the orbits of two spacecraft by making measurements of the vector from one spacecraft position to the other. To make the two orbits observable, this vector must be referenced to inertial space, and a time series of these measurements is needed.

All of the sensors for the proposed system could reside on one of the spacecraft. Call the instrumented spacecraft spacecraft A and the other spacecraft spacecraft B. Spacecraft A would need a 3-axis star sensor system to determine its inertial attitude, and it would need instrumentation to measure the relative position vector of spacecraft B. The relative position measurement could be made by a laser range finder and an optical telescope, the former for measuring distance and the latter for measuring direction. Spacecraft B could be a dumb drone, perhaps just a metal sphere with suitable coating to reflect both spacecraft A's laser range finder signal and enough sunlight to make it visible to spacecraft A's optical system. Reference 8 describes an alternative system for measuring spacecraft B's relative position. It has additional capabilities, but it is likely to have poorer range accuracy.

A number of other researchers have studied spacecraft-to-spacecraft range measurements to enhance orbit determination capabilities for a constellation of spacecraft.[9–11] The orbits are not all independently observable in this case because a simultaneous rigid-body-type motion of the entire constellation does not affect relative range.[9] Such techniques only help to reduce drift.

In Ref. 12, many different measurement sets for autonomous orbit determination of high altitude spacecraft are considered, including range and inertially referenced angles from one spacecraft to another. The difference between that study and the present one is that in Ref. 12 spacecraft B is considered to have a known orbit and position.

Markley,[7] in the appendix of his paper, showed that the two orbits of the proposed system are absolutely observable except for certain special orbital configurations. One important unobservable case is that of two spacecraft in coplanar circular orbits with the same semimajor axis. His analysis considered only the $1/r^2$ gravitational force. It demonstrated mathematical observability without calculating covariances or predicting accuracy. Markley's paper concludes by stating that the next study of this system should investigate achievable accuracies and their dependence on system configuration.

The present study makes four contributions. First, it explains the system's observability. Second, it shows that the secular J_2 effects make some of Markley's unobservable cases observable. Third, it calculates covariances based on measurement errors to predict a lower bound on orbit estimation error, and fourth, it explores how these covariances vary with configuration and system parameters, such as spacecraft separation and sensor accuracy.

The remainder of this paper consists of four sections and conclusions. Section II uses physics and geometry to partially explain why the two spacecraft orbits are simultaneously observable. Section III describes dynamics and measurement models, a batch filter, and a covariance analysis that will be used to study observability and accuracy. Section IV presents the covariance analysis results. Section V presents some additional results and discusses operational and design issues associated with this system. Section VI gives the conclusions.

II. Physical/Geometrical Explanation of System Observability

Getting an Earth Reference: A Gravity Gradiometer Analogy

Systems for autonomous Earth orbit determination rely on measuring inertial attitude and the vector or direction to some nearby object, such as the Earth or the moon.[5] The Earth is the most commonly used nearby object. Its nearness increases the position accuracy that is achievable for a given sensor accuracy. Three basic methods exist for using the Earth as a reference: horizon sensing at CO_2 emission wavelengths, refraction of light from nearly occulted stars, and tracking of landmarks. Each of these methods has significant limitations.

Another way to get an Earth reference is through use of the Earth's gravity gradient.[13] The 3×3 gravity gradient tensor matrix G is the derivative of the gravitational acceleration vector with respect to displacement: $G = \mathrm{d}\boldsymbol{g}/\mathrm{d}\boldsymbol{r}$, where $\boldsymbol{g}$ is the gravitational acceleration vector and $\boldsymbol{r}$ is the position at which the acceleration is measured.

Received Jan. 8, 1998; revision received Aug. 3, 1998; presented as Paper 98-4560 at the AIAA/AAS Astrodynamics Specialist Conference, Boston, MA, Aug. 10–12, 1998; accepted for publication Oct. 24, 1998.

*Associate Professor, Sibley School of Mechanical and Aerospace Engineering. Associate Fellow AIAA.

For a simple $1/\|\boldsymbol{r}\|^2$ gravitational field, the gravity gradient matrix is

$$G = -\frac{\mu}{(\boldsymbol{r}^T\boldsymbol{r})^{5/2}}[(\boldsymbol{r}^T\boldsymbol{r})I - 3\boldsymbol{r}\boldsymbol{r}^T] \tag{1}$$

where μ is the geocentric gravitational constant. Given this tensor in a spacecraft coordinate system, it is straightforward to determine the $\boldsymbol{r}$ vector in that coordinate system, up to a sign.

There exist instruments to measure the gravity gradient.[14] Conceptually, a gravity gradiometer consists of an array of very sensitive accelerometers that are arranged on a spatial grid. The accelerometer outputs are differenced to determine the spatial derivatives of the acceleration field.

A gradiometer is difficult to make and use in practice. For array dimensions that would fit into a practical spacecraft, a gradiometer requires accelerometers with an extremely large dynamic range. Furthermore, spacecraft-generated gravity gradients can be significant.

The present system can be thought of as a very long baseline gravity gradiometer. The two spacecraft are the proof masses of two accelerometers in a gravity gradiometer. Their separation is the baseline of the gradiometer. The relative position measurements can be differentiated to determine the relative acceleration. A nonzero relative acceleration is caused by the Earth's gravity gradient. This gravity gradient depends on the position of the midpoint between the two spacecraft, which is why the system yields a signal that can be used for orbit/position determination. The use of two independent spacecraft as the proof masses allows for large gradiometer baselines, and all of the problems with gradiometers essentially go away for large enough baselines.

Admittedly, this gravity gradiometer analogy is not perfect. This system does not measure all of the elements of the G matrix, and changes in the orientation of the baseline between the two spacecraft cause the gradiometer's sensing axis to vary with time. Also, higher-order gravity gradient terms become significant as the baseline's length increases. Nevertheless, this system can use the gravity field's variations to get a very good Earth reference.

Geometric Observability of the Planar Keplerian Elements

One can understand the observability of the proposed system by considering orbital geometry. First, consider the planar case for orbits in a simple $1/r^2$ gravitational field. Suppose that the two spacecraft orbits are in the same plane and that each is defined by four Kepler elements: the mean anomaly at epoch M_0, the mean motion M_1, the eccentricity e, and the argument of perigee ω. (Note: a more standard notation would use n in place of M_1.) The mean motion is related to the mean semimajor axis a by the relationship $M_1^2 a^3 = \mu$. The semimajor axis and the eccentricity are related to the semiminor axis b by the relationship $b^2 = a^2(1-e^2)$. Figure 1 shows the orbit of a single spacecraft, the geometric definitions of a, b, and ω, and the true anomaly at epoch ν_0, which is a function of the mean anomaly at epoch and the eccentricity: $\nu_0 = \nu(M_0, e) = M_0 + \mathcal{O}(e)$ (Ref. 15).

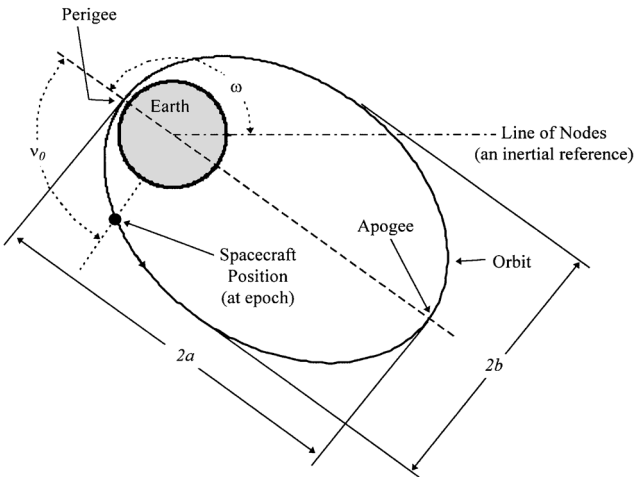

Fig. 1 Kepler elements of a planar orbit.

The measurement that will be used to determine the spacecraft orbits is the inertially referenced relative position vector between spacecraft A and spacecraft B, $\boldsymbol{r}_{BA}$. Figure 2 shows a sequence of locations of this vector as the two spacecraft travel around their respective orbits. As shown by Fig. 2, this vector can vary with time in two distinct ways: Its inertial direction ψ_{BA} can change with time, and its length $\rho_{BA} = \|\boldsymbol{r}_{BA}\|$ can change with time.

The remainder of this section will show how the time histories of the direction and length of $\boldsymbol{r}_{BA}$ are locally unique functions of the four Kepler elements of the two spacecraft. To do this, small perturbations to a nominal situation will be considered. The nominal situation is that of two spacecraft in the same orbit but with different values of M_0 so that there is a difference in where they are along the orbit. The nominal orbit is nearly circular, with an apogee altitude of 585 km and a perigee altitude of 515 km. The spacecraft are nominally separated by about 100 km, with spacecraft B leading spacecraft A around the orbit. A perturbation of the orbital elements will produce perturbations in $\rho_{BA}(t)$ and in $\psi_{BA}(t)$. Call these perturbations $\Delta\rho_{BA}(t)$ and $\Delta\psi_{BA}(t)$.

In the discussion that follows (and in the remainder of the paper) a subscript A on a Kepler element indicates that it belongs to orbit A, and a subscript B indicates orbit B. Thus, M_{0A} is the mean anomaly at epoch of orbit A, and M_{1B} is the mean motion of orbit B.

Consider why M_{0A} and M_{0B} are simultaneously observable. If they are perturbed so that $\Delta M_{0A} = -\Delta M_{0B}$, i.e., so that both spacecraft are perturbed along their respective orbits in opposite directions, then $\Delta\rho_{BA}(t)$ is a nonzero, approximately constant perturbation whereas $\Delta\psi_{BA}(t) \cong 0$. If, on the other hand, $\Delta M_{0A} = +\Delta M_{0B}$, which perturbs both spacecraft in the same direction along their respective orbits, then $\Delta\rho_{BA}(t) \cong 0$, and $\Delta\psi_{BA}(t)$ is nonzero and approximately constant. These two situations can be distinguished from each other based on the unique ways in which they perturb the $\rho_{BA}(t)$ and $\psi_{BA}(t)$ responses (Fig. 3).

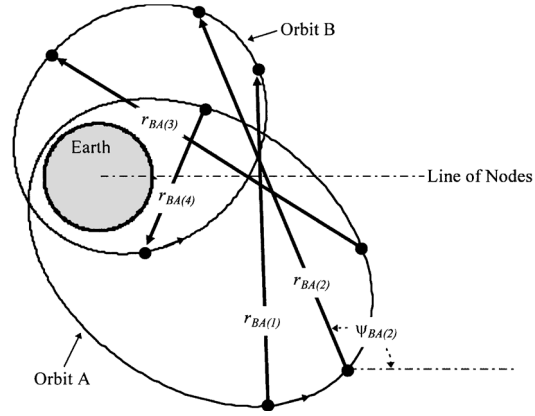

Fig. 2 Four locations of two spacecraft and their relative positive vector, the planar case.

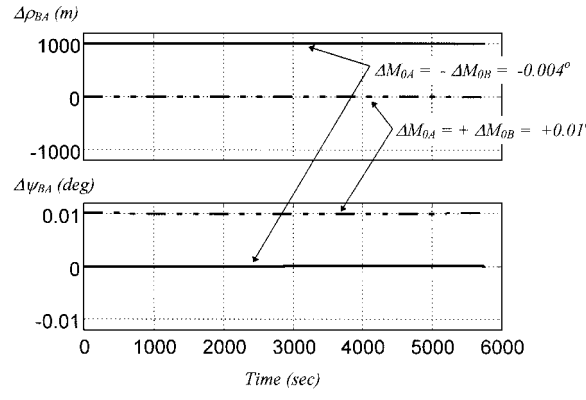

Fig. 3 Effects of ΔM_{0A} and ΔM_{0B} on the perturbation time histories $\Delta\rho_{BA}(t)$ and $\Delta\psi_{BA}(t)$.

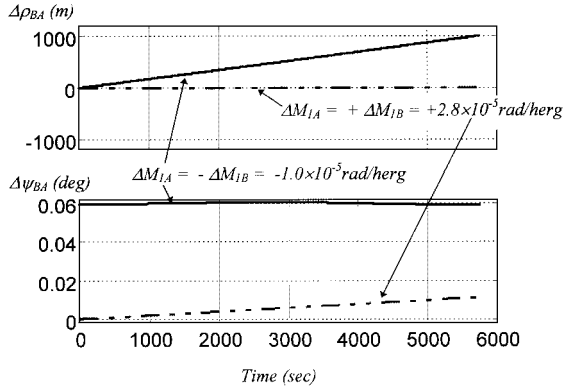

Fig. 4 Perturbation time histories of $\Delta\rho_{BA}(t)$ and $\Delta\psi_{BA}(t)$ that are caused by combinations of ΔM_{1A} and ΔM_{1B}.

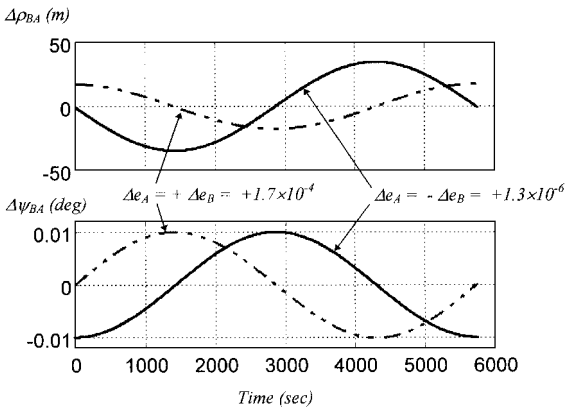

Fig. 5 $\Delta\rho_{BA}(t)$ and $\Delta\psi_{BA}(t)$ perturbation time histories that result from two linearly independent combinations of Δe_A and Δe_B.

Perturbations in M_{1A} and M_{1B} produce ramps in $\Delta\rho_{BA}(t)$ and $\Delta\psi_{BA}(t)$. If $\Delta M_{1A} = -\Delta M_{1B}$, then the two spacecraft orbit the Earth with different periods. The difference of orbital periods causes the length of $\boldsymbol{r}_{BA}$ to change with time so that $\Delta\rho_{BA}(t)$ is a ramp. This change also causes a roughly constant $\Delta\psi_{BA}(t)$ perturbation due to the difference in altitudes that results from the difference in semimajor axes. If $\Delta M_{1A} = +\Delta M_{1B}$, then the two spacecraft orbit together but at a different common orbital rate. This gives rise to a ramping $\Delta\psi_{BA}(t)$ and leaves $\Delta\rho_{BA}(t) \cong 0$. Figure 4 shows $\Delta\rho_{BA}(t)$ and $\Delta\psi_{BA}(t)$ for these two perturbation cases. Obviously, these two cases can be distinguished from each other and from the cases associated with Fig. 3.

The simultaneous observability of the two spacecraft's eccentricities is more difficult to understand. Perturbation of each eccentricity causes once-per-orbit oscillations of $\Delta\rho_{BA}(t)$ and $\Delta\psi_{BA}(t)$. Figure 5 shows the 1-orbit $\Delta\rho_{BA}(t)$ and $\Delta\psi_{BA}(t)$ responses for two linearly independent eccentricity perturbations, one in which $\Delta e_A = -\Delta e_B$ and the other in which $\Delta e_A = +\Delta e_B$. Figure 5 shows distinct phase differences for the two cases, which make them distinguishable from each other based on response measurements. These cases are distinguishable from the cases associated with Figs. 3 and 4 because neither of those figures shows an oscillatory response.

Consider perturbations $\Delta\omega_A$ and $\Delta\omega_B$ with simultaneous perturbations of M_{0A} and M_{0B} such that $\Delta M_{0A} = -\Delta\omega_A$ and $\Delta M_{0B} = -\Delta\omega_B$. Any two linearly independent perturbations of this type cause once-per-orbit oscillations that are distinguishable from each other and from the oscillations that are caused by perturbations of e_A and e_B. They are distinguishable from each other because of a 90-deg phase difference, as in the case of linearly independent Δe_A and Δe_B perturbations. They are distinguishable from Δe_A and Δe_B perturbations because they give rise to different phase and amplitude relationships between the $\Delta\rho_{BA}(t)$ signal and the $\Delta\psi_{BA}(t)$ signal than are caused by Δe_A and Δe_B perturbations.

In summary, the eight planar Kepler elements are independently observable because eight linearly independent element perturbations give rise to eight independent $\Delta\rho_{BA}(t)$ and $\Delta\psi_{BA}(t)$ time histories.

Geometric Observability of the Orbital Planes

The observability of the two orbital planes is partly explainable from geometry. First, suppose that both spacecraft are in the same orbital plane. Then $\boldsymbol{r}_{BA}$ stays in that plane, rotating and changing length. The rotations are all about the orbit normal vector. The cross product of $\boldsymbol{r}_{BA}$ with its time derivative indicates the orbit normal, which defines the orbital plane.

The case of noncoplanar orbits is more complicated. Suppose that the two orbital planes are near each other. One might hope that the time average of $\boldsymbol{r}_{BA} \times \{d\boldsymbol{r}_{BA}/dt\}$ would define the normal to an average orbital plane. If the $\boldsymbol{r}_{BA}$ vector had a component that was perpendicular to this average orbital plane, then this out-of-plane component would oscillate. Its oscillation amplitude would determine the separation between the two spacecraft orbital planes, and its oscillation phase would determine where the two planes intersected. This information would be sufficient to uniquely determine both orbital planes.

Unfortunately, the actual situation is more complicated. If there is just a $1/r^2$ gravitational force, then the preceding explanation has a weakness: To first order in the orbital separation, the vector $\boldsymbol{r}_{BA}$ can remain in a single plane even though the two orbits are in slightly different planes. This occurs when the two spacecraft have the same apogee and perigee and reach them at the same time.[7] As will be demonstrated, the secular effects of the J_2 gravity term induce observability in this case, but it is not straightforward to explain geometrically why the system becomes observable with J_2 effects.

III. System Model, Batch Filter Design, and Covariance Analysis Technique

System Model

A system model can be used to mathematically demonstrate observability, to develop a filter for estimating the orbits from data, and to predict the filter's estimation error covariance.

Estimation Vector

The estimation vector for this study has 14 elements, 6 Kepler elements plus a drag parameter for each spacecraft. It is

$$\boldsymbol{p} = [M_{0A}, M_{1A}, M_{2A}, e_A, \omega_{0A}, \lambda_{0A}, i_A, M_{0B}, M_{1B}, M_{2B}, e_B, \omega_{0B}, \lambda_{0B}, i_B]^T \tag{2}$$

where M_2 is the drag parameter, ω_0 is the argument of perigee at epoch, λ_0 is the longitude of the ascending node at epoch, and i is the inclination. The epoch time is defined as $t = 0$.

The $\boldsymbol{p}$ vector contains no bias or misalignment estimates. In practice, all of the sensors that would be used in the proposed system might have biases, misalignments, or both. Depending on the sensor characteristics, there might even be a slow drift in these error sources. If not corrected, such measurement errors would degrade system performance because some of the orbital elements' effects on the data also appear as biases or drifts. For example, a range sensor bias error would alias into errors in M_{0A} and M_{0B} of equal magnitude but opposite sign (review Fig. 3), whereas an orientation sensor drift error would alias into equal errors in M_{1A} and M_{1B} (review Fig. 4).

The analysis that follows assumes that the spacecraft would undergo a calibration period, during which additional sensor data would be available, such as ground-tracking data. This additional data would be used to determine any important biases, misalignments, and drift rates that otherwise would be unobservable. The accuracy of the system after calibration would be directly dependent on the accuracy with which these calibrations could be extrapolated.

Model of Orbital Motion

The observability of the proposed system depends on there being an accurate model of the orbital motion of each spacecraft. This study uses a dynamic model that is based on physics. It gives each

spacecraft's geocentric position as a function of time and orbital state

$$\theta = \theta(t;\, M_0, M_1, M_2, e, \omega_0, \lambda_0, i) \tag{3a}$$

$$\phi = \phi(t;\, M_0, M_1, M_2, e, \omega_0, \lambda_0, i) \tag{3b}$$

$$r = r(t;\, M_0, M_1, M_2, e, \omega_0, \lambda_0, i) \tag{3c}$$

where t is the time since epoch, θ is the colatitude, ϕ is the longitude, and r is the geocentric radius, all measured with respect to a rotating, Earth-fixed coordinate system. The equations that define this model come from the appendix of Ref. 15 and are omitted for the sake of brevity.

The following physics are included in the model.[15] The $1/r^2$ gravitational force is the main force. The motions are modeled as Keplerian motions with small perturbations due to drag and higher-order gravity effects. Secular drag effects on the mean motion and on the semimajor axis are included by using the model $M(t) = M_0 + M_1 t + M_2 t^2$, but the secular drag effect on the decay of the eccentricity is not included. The secular J_2 effects on the argument of perigee and on the longitude of the ascending node are included as are the J_2 effects on the relationship between the mean motion and the semimajor axis.

This paper will present filter accuracy results that are orders of magnitude more accurate than this orbital dynamics model. In practice, this model is only accurate to about 6 km when propagated over a single low Earth orbit with perfectly known initial position and velocity. Although it seems inconsistent to quote more accuracy than the dynamic model can achieve, the use of an inaccurate model for a covariance study is justified by the following philosophy: The basic model features that make the system observable are contained in this crude orbital model. Therefore, a more accurate dynamic model would not make the system more or less observable in the mathematical sense. Therefore, it is not worth the effort to incorporate a high-fidelity model at this stage of the investigation.

If a high-fidelity model exists that can propagate the orbit to the accuracy that the filter purports to achieve, then the filter's purported accuracy can be achieved with real flight data simply by replacing its dynamic model with the high-fidelity model. This is true even though some of the effects that are neglected by the current model may produce perturbation time histories such as those shown in Figs. 3–5. If the present low-fidelity model were used on real flight data, then the similarity between neglected effects and orbit-element perturbations would have a large negative impact on accuracy. Given a filter with more realistic gravity, drag, and other effects, however, the impact on accuracy would vanish because perturbational effects such as those in Figs. 3–5 do not change significantly for higher-fidelity orbital models.

Model of Measurements

The measurement model defines the sensor measurements, their error statistics, and their dependence on $\boldsymbol{p}$.

The basic measurement is the $\boldsymbol{r}_{BA}$ vector referenced to inertial coordinates. The error statistics depend on how the vector is measured. Most likely, its length would be measured by a radio-wave-based or laser-based ranging system. Its direction would be measured by some other system, possibly an optical telescope. Directional accuracy would be affected by inaccuracy of the inertial attitude determination system.

The measurement vector $\boldsymbol{r}_{BA}$ has been decomposed into length and directional measurements. Suppose that $\boldsymbol{r}_{BA\,\mathrm{meas}(k)}$ is the measured value of $\boldsymbol{r}_{BA}$ at sample time t_k and that $\hat{\boldsymbol{q}}_{2(k)}$ and $\hat{\boldsymbol{q}}_{3(k)}$ are any two unit vectors that are perpendicular to each other and to $\boldsymbol{r}_{BA\,\mathrm{meas}(k)}$. Suppose, also, that $\rho_{BA\,\mathrm{meas}(k)} = \sqrt{[r^T_{BA\,\mathrm{meas}(k)} r_{BA\,\mathrm{meas}(k)}]}$. Then the measurement model is

$$\rho_{BA\,\mathrm{meas}(k)} = \rho_{BA(k)} + n_{\rho(k)} \tag{4a}$$

$$0 = \hat{\boldsymbol{q}}^T_{2(k)} \boldsymbol{r}_{BA(k)} + n_{2(k)} \tag{4b}$$

$$0 = \hat{\boldsymbol{q}}^T_{3(k)} \boldsymbol{r}_{BA(k)} + n_{3(k)} \tag{4c}$$

where $n_{\rho(k)}$ is the length error and $n_{2(k)}$ and $n_{3(k)}$ are directional errors. The unit vectors $\hat{\boldsymbol{q}}_{2(k)}$ and $\hat{\boldsymbol{q}}_{3(k)}$ are arbitrary, but their directions vary with time to remain perpendicular to $\boldsymbol{r}_{BA}$ and to each other. The errors $n_{\rho(k)}$, $n_{2(k)}$, and $n_{3(k)}$ are assumed to be Gaussian random sequences and to have statistics

$$E\{n_{\rho(k)}\} = 0, \qquad E\{n_{\rho(j)} n_{\rho(k)}\} = \sigma^2_{\mathrm{mag}} \delta_{jk} \tag{5a}$$

$$E\{n_{i(k)}\} = 0, \qquad E\{n_{i(j)} n_{i(k)}\} = \sigma^2_{\mathrm{dir}(k)} \delta_{jk}, \qquad \text{for } i = 2, 3 \tag{5b}$$

$$E\{n_{2(j)} n_{3(k)}\} = 0, \qquad E\{n_{\rho(j)} n_{i(k)}\} = 0, \qquad \text{for } i = 2, 3 \tag{5c}$$

where $\sigma_{\mathrm{dir}(k)} = \max\{(\rho_{BA\,\mathrm{meas}(k)} \cdot \sigma_{\mathrm{ang}}), \sigma_{\mathrm{dirmin}}\}$. In these equations σ_{mag} is the standard deviation (in meters) of the length measurement error, σ_{ang} is the standard deviation (in radians) of the direction measurement error, and σ_{dirmin} is a minimum direction error (in meters). Note how σ_{ang} gets multiplied by $\rho_{BA\,\mathrm{meas}(k)}$ to transform it into a length, consistent with the definitions of $n_{2(k)}$ and $n_{3(k)}$. The quantity σ_{dirmin} models the limiting effects of finite spacecraft size on directional accuracy for very small separations between the two spacecraft.

The next part of the measurement model computes a modeled value $\boldsymbol{r}_{BA(k)}$ as a function of the $\boldsymbol{p}$ estimation vector. Using the following definitions:

$$\theta_{A(k)}(\boldsymbol{p}) = \theta\left(t_{(k)};\, M_{0A}, M_{1A}, M_{2A}, e_A, \omega_{0A}, \lambda_{0A}, i_A\right) \tag{6a}$$

$$\phi_{A(k)}(\boldsymbol{p}) = \phi\left(t_{(k)};\, M_{0A}, M_{1A}, M_{2A}, e_A, \omega_{0A}, \lambda_{0A}, i_A\right) \tag{6b}$$

$$r_{A(k)}(\boldsymbol{p}) = r\left(t_{(k)};\, M_{0A}, M_{1A}, M_{2A}, e_A, \omega_{0A}, \lambda_{0A}, i_A\right) \tag{6c}$$

$$\theta_{B(k)}(\boldsymbol{p}) = \theta\left(t_{(k)};\, M_{0B}, M_{1B}, M_{2B}, e_B, \omega_{0B}, \lambda_{0B}, i_B\right) \tag{6d}$$

$$\phi_{B(k)}(\boldsymbol{p}) = \phi\left(t_{(k)};\, M_{0B}, M_{1B}, M_{2B}, e_B, \omega_{0B}, \lambda_{0B}, i_B\right) \tag{6e}$$

$$r_{B(k)}(\boldsymbol{p}) = r\left(t_{(k)};\, M_{0B}, M_{1B}, M_{2B}, e_B, \omega_{0B}, \lambda_{0B}, i_B\right) \tag{6f}$$

the modeled $\boldsymbol{r}_{BA}$ function is

$$\boldsymbol{r}_{BA\,\mathrm{mod}(k)}(\boldsymbol{p}) = \begin{bmatrix} \left\{r_{B(k)} \sin\theta_{B(k)} \cos\left(\phi_{B(k)} + \gamma_{(k)}\right) - r_{A(k)} \sin\theta_{A(k)} \cos\left(\phi_{A(k)} + \gamma_{(k)}\right)\right\} \\ \left\{r_{B(k)} \sin\theta_{B(k)} \sin\left(\phi_{B(k)} + \gamma_{(k)}\right) - r_{A(k)} \sin\theta_{A(k)} \sin\left(\phi_{A(k)} + \gamma_{(k)}\right)\right\} \\ \left\{r_{B(k)} \cos\theta_{B(k)} - r_{A(k)} \cos\theta_{A(k)}\right\} \end{bmatrix} \tag{7}$$

where $\gamma_{(k)}$ is the Greenwich hour angle at time $t_{(k)}$. This vector is referenced to Earth-centered inertial coordinates, as required.

The measured and modeled $\boldsymbol{r}_{BA}$ vectors are used to derive error equations that can be used in filtering and in covariance/observability analysis. The error equations are derived by substituting the modeled value of $\boldsymbol{r}_{BA}$ into Eqs. (4a–4c), solving for the measurement errors, and normalizing the errors by their standard deviations:

$$\eta_{1(k)}(\boldsymbol{p}) = \frac{\left[\rho_{BA\,\mathrm{meas}(k)} - \rho_{BA\,\mathrm{mod}(k)}(\boldsymbol{p})\right]}{\sigma_{\mathrm{mag}}} \tag{8a}$$

$$\eta_{2(k)}(\boldsymbol{p}) = \frac{\left[-\hat{q}^T_{2(k)} \boldsymbol{r}_{BA\,\mathrm{mod}(k)}(\boldsymbol{p})\right]}{\sigma_{\mathrm{dir}(k)}} \tag{8b}$$

$$\eta_{3(k)}(\boldsymbol{p}) = \frac{\left[-\hat{q}^T_{3(k)} \boldsymbol{r}_{BA\,\mathrm{mod}(k)}(\boldsymbol{p})\right]}{\sigma_{\mathrm{dir}(k)}} \tag{8c}$$

The normalized measurement errors that are defined by these equations, $\eta_{i(k)}$ for $i = 1, 2, 3$, have zero mean and unit variance, according to the statistical model.

There are two possible forms of the length model $\rho_{BA\,\mathrm{mod}(k)}(\boldsymbol{p})$ that can get used in Eq. (8a):

$$\rho_{BA\,\mathrm{mod}(k)}(\boldsymbol{p}) = \frac{\boldsymbol{r}^T_{BA\,\mathrm{meas}(k)}\boldsymbol{r}_{BA\,\mathrm{mod}(k)}(\boldsymbol{p})}{\sqrt{\boldsymbol{r}^T_{BA\,\mathrm{meas}(k)}\boldsymbol{r}_{BA\,\mathrm{meas}(k)}}} \tag{9}$$

or

$$\rho_{BA\,\mathrm{mod}(k)}(\boldsymbol{p}) = \sqrt{\boldsymbol{r}^T_{BA\,\mathrm{mod}(k)}(\boldsymbol{p})\,\boldsymbol{r}_{BA\,\mathrm{mod}(k)}(\boldsymbol{p})} \tag{10}$$

The first form is the projection of $\boldsymbol{r}_{BA\,\mathrm{mod}(k)}(\boldsymbol{p})$ along $\boldsymbol{r}_{BA\,\mathrm{meas}(k)}(\boldsymbol{p})$. This form provides better convergence in a nonlinear least-squares batch filter. The second form is the actual length of the $\boldsymbol{r}_{BA\,\mathrm{mod}(k)}(\boldsymbol{p})$ vector. For small values of the angular direction error σ_{ang}, both forms produce similar results. Therefore, the first is to be preferred because of its better convergence. For large values of σ_{ang}, however, the second form of the length measurement is preferred because it yields a smaller filter covariance and better consistency between the actual residuals' statistics and the modeled statistics.

Nonlinear Least-Squares Batch Filter

A batch filter based on nonlinear least squares provides one technique for deducing a $\boldsymbol{p}$ estimation vector from a measurement sequence, $\boldsymbol{r}_{BA\,\mathrm{meas}(1)}, \boldsymbol{r}_{BA\,\mathrm{meas}(2)}, \boldsymbol{r}_{BA\,\mathrm{meas}(3)}, \ldots, \boldsymbol{r}_{BA\,\mathrm{meas}(N)}$. This filter finds the value of $\boldsymbol{p}$ that minimizes the nonlinear least-squares cost function

$$J(\boldsymbol{p}) = \frac{1}{2}\sum_{k=1}^{N}\left\{\sum_{i=1}^{3}\left[\eta_{i(k)}(\boldsymbol{p})\right]^2\right\} \tag{11}$$

which is the sum over all of the sample instants of the squares of the measurement errors.

Standard iterative gradient-based techniques exist to solve for a locally minimizing value of the $\boldsymbol{p}$ vector.[16] A restricted-step-length Gauss–Newton method has been used here.

A batch filter has been used instead of an extended Kalman filter because it is more consistent with the covariance/system-observability analysis that will be described and because its software had already been adapted to orbit determination. A weakness of this filter is that the statistical effects of random process disturbances are not included in its model.

Statistical Interpretation and Covariance Analysis

The error equations (8a–8c) lead to a statistical interpretation of the batch filter's estimation error. Taken over all samples from 1 to N, the error equations take the form

$$0 = \boldsymbol{\eta}(\boldsymbol{p}) = \begin{bmatrix} \eta_{1(1)}(\boldsymbol{p}) \\ \eta_{2(1)}(\boldsymbol{p}) \\ \eta_{3(1)}(\boldsymbol{p}) \\ \vdots \\ \eta_{1(N)}(\boldsymbol{p}) \\ \eta_{2(N)}(\boldsymbol{p}) \\ \eta_{3(N)}(\boldsymbol{p}) \end{bmatrix} \tag{12}$$

The least-squares cost function in Eq. (11) is the sum of the squared errors of these equations.

The Jacobian of the error equations is

$$A = \frac{\partial \boldsymbol{\eta}}{\partial \boldsymbol{p}} = \begin{bmatrix} -\dfrac{1}{\sigma_{\mathrm{mag}}}\dfrac{\partial \rho_{BA\,\mathrm{mod}(1)}}{\partial \boldsymbol{p}} \\ -\dfrac{1}{\sigma_{\mathrm{dir}(1)}}\hat{\boldsymbol{q}}^T_{2(1)}\dfrac{\partial \boldsymbol{r}_{BA\,\mathrm{mod}(1)}}{\partial \boldsymbol{p}} \\ \vdots \\ -\dfrac{1}{\sigma_{\mathrm{dir}(N)}}\hat{\boldsymbol{q}}^T_{3(N)}\dfrac{\partial \boldsymbol{r}_{BA\,\mathrm{mod}(N)}}{\partial \boldsymbol{p}} \end{bmatrix} \tag{13}$$

This Jacobian must have full column rank for the system to be observable in the local linearized sense.

The Jacobian determines the covariance matrix of the batch filter's $\boldsymbol{p}$ estimation error

$$P_{pp} = E\left\{(\boldsymbol{p} - \boldsymbol{p}_{\mathrm{est}})(\boldsymbol{p} - \boldsymbol{p}_{\mathrm{est}})^T\right\} = (A^T A)^{-1} \tag{14}$$

The covariance of $\boldsymbol{p}$ is finite if and only if the system is observable because $A^T A$ is the system's observability Gramian, and it is nonsingular if and only if the system is observable.

A practical test of observability is to test the size of the elements of P_{pp}. Strict mathematical observability holds if these are all finite, but very large values indicate that the system is near to being unobservable, so near that the filter's estimates will be useless. Therefore, practical observability is investigated by considering the size of the covariance matrix.

There is a problem in determining what constitutes bigness or smallness of an element of the P_{pp} matrix. These elements are covariances of Kepler parameters. The relationship between estimation errors in Kepler parameters and spacecraft position estimation errors is nonlinear and complicated.

The solution to this problem is to characterize the size of a given P_{pp} covariance matrix by the resulting standard deviations of spacecraft position estimates. These standard deviations are functions of P_{pp} and of the time since epoch. The along-track, across-track, and altitude standard deviation functions are defined in Eqs. (11) and (12) of Ref. 15. For a given data batch, these position component standard deviations vary with time over the batch interval. This paper uses the maximum of each component's standard deviation over the batch interval as a measure of estimated spacecraft position accuracy.

IV. Covariance Analysis Results

The system's predicted covariance has been calculated for a number of different cases. These cases explore the effects of spacecraft separation, spacecraft relative position, orbital parameters, and sensor accuracy. It is helpful to begin by presenting the results of a typical case. This case will be used as a baseline for analyzing the effects of various parameter changes.

The baseline case is for both spacecraft in low Earth orbits (LEO) such that they stay within 150 km of each other at all times. Both orbits are nearly circular, both having an apogee altitude of 585 km and a perigee altitude of 515 km. Spacecraft B leads spacecraft A by an along-track separation that varies between 97.8 and 99.8 km. The orbital planes are slightly different so that the maximum across-track separation is just 92.8 km. The assumed sensor error statistics are $\sigma_{\mathrm{mag}} = 0.1$ m rms range error, $\sigma_{\mathrm{ang}} = 0.2$ arcsec rms direction error, and $\sigma_{\mathrm{dirmin}} = 0.1$ m minimum rms error perpendicular to $\boldsymbol{r}_{BA}$. A data batch of $N = 1501$ samples is used with an intersample spacing of $t_{k+1} - t_k = 3.83$ s. The batch interval equals one orbital period.

The orbit determination accuracy for this case is very good. The maximum along-track, across-track, and altitude standard deviations for spacecraft A are 1.27, 0.64, and 0.82 m, respectively. The results for spacecraft B are essentially identical, and the similarity of results for the two spacecraft carries over into all of the cases that have been run, with one exception. Therefore, only spacecraft A's standard deviations will be reported for most cases.

Figure 6 shows spacecraft A's position component standard deviations as functions of time for the batch interval. These are the standard deviations implied by the covariance of the estimated $\boldsymbol{p}$ vector, P_{pp}. The values 1.27, 0.64, and 0.82 m are the respective maxima of the three curves of Fig. 6.

The elements of the P_{pp} covariance matrix also show good accuracy. Most of the standard deviations associated with angles are on the order of 10^{-8} rad, with the standard deviations of the two perigee locations on the order of 10^{-6} rad. The mean motion M_1 and the eccentricity, e are well determined for both spacecraft: The ratios of the M_1 standard deviations to their actual values are 1.3×10^{-7}, and the ratios of the e standard deviations to their actual values are 7.8×10^{-6}. The least-accurate quantities are M_{2A} and M_{2B}. Their standard deviations are 12% of their actual values. The M_2 uncertainty is the dominant effect in the along-track direction, and its effect on the maximum altitude uncertainty is significant.

Table 1 Spacecraft A position standard deviations as functions of system parameters for LEO

Case	$r_{BA(\text{along-track})}$, km minimum	$r_{BA(\text{along-track})}$, km maximum	$\lvert r_{BA(\text{across-track})}\rvert$, km maximum	σ_{ang}, arcsec	$(t_{k+1} - t_k)$, s	Maximum component σ, m A-T	C-T	Altitude
1	97.8	99.8	92.8	0.2	3.83	1.27	0.64	0.82
2	9.8	10.0	9.3	0.2	3.83	12.1	5.71	7.62
3	945.1	1019.0	925.7	0.2	3.83	0.54	0.28	0.48
4	99.6	100.6	0.0	0.2	3.83	1.20	234.3	1.13
5	−0.4	0.4	100.2	0.2	3.83	287.6	2.13	4.53
6	−39.9	240.0	0.0	0.2	3.83	1.14	1.02	1.20
7	96.2	99.8	92.8	0.2	7.66	0.70	0.43	0.23
8	97.8	99.8	92.8	2.0	3.83	5.33	2.80	4.60

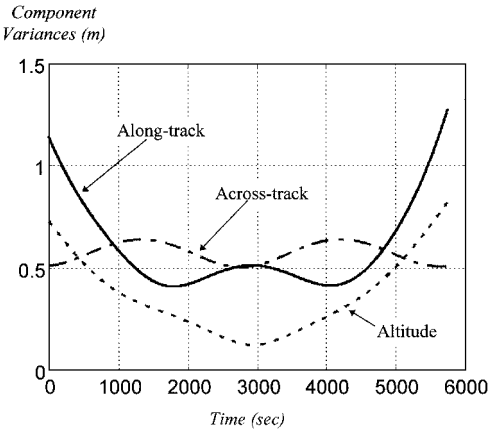

Fig. 6 Spacecraft A's three position component standard deviations as functions of time, a typical case.

Some of the correlation coefficients in the P_{pp} matrix have magnitudes very near to unity. The largest ones are the correlations between similar quantities for the two different spacecraft. For example, the correlation between M_{0A} errors and M_{0B} errors is very nearly 1. These high correlation coefficients do not indicate poor observability. Rather, they indicate that certain directions in the $\boldsymbol{p}$ estimation vector space are more observable than others. The directions associated with the interspacecraft separation are the most observable due to the form of the measurements. If an appropriate change of coordinates is used, one that replaces quantities like M_{0A} and M_{0B} with the linear combinations $\{M_{0A} + M_{0B}\}$ and $\{M_{0A} - M_{0B}\}$, then all near-unity correlation coefficients disappear from the covariance matrix.

These results prove that this system is practically observable. Its observability Gramian, A^TA, is nonsingular, and the A^TA condition number is small enough to yield good accuracy.

This case and various other cases are summarized in Table 1. In each case of Table 1, the two spacecraft orbits have the same apogee and perigee altitudes: 585 and 515 km. Also, all cases use the sensor accuracies $\sigma_{\text{mag}} = \sigma_{\text{dirmin}} = 0.1$ m, and in all cases $N = 1501$. Case 1 corresponds to the nominal case that has just been described. The other cases are discussed subsequently. The last three columns in Table 1 report the maximum along-track (A-T), across-track (C-T), and altitude standard deviations for spacecraft A's estimated orbit.

An important characteristic of the system is the distance between the spacecraft. Two cases have been run that are identical to the nominal case except that the spacecraft are closer to each other by a factor of 10 in one case and farther away by a factor of 10 in the other case. The cases are, respectively, cases 2 and 3 of Table 1. Based on the gravity-gradient analogy, one would expect the accuracy to decrease when baseline separation between the proof masses decreases and to increase when the separation increases. This is exactly the situation: Case 2 is about 10 times less accurate than case 1, whereas case 3 is about twice as accurate as case 1. Compare the three position component standard deviation maxima for these three cases. Case 2 suffers a dramatic loss of accuracy because the baseline decreases while all of the sensor accuracies remain constant; σ_{dir} for case 2 is comparable to σ_{dir} for case 1 because it is already near σ_{dirmin} for case 1. Case 3's accuracy increases, but not by as much as one would expect based on cases 1 and 2. This happens because σ_{dir} increases for case 3 due to its $\sigma_{\text{ang}} \cdot \rho_{BA}$ dependence.

A significant characteristic is the relationship of the separation vector's orientation to the two orbits. If the two spacecraft are near each other and in similar orbits, then the best accuracy is achieved in either of two situations. One occurs when there is significant maximum along-track separation and significant maximum across-track separation. The other occurs when there is eccentricity and the perigee of one orbit is in phase with the apogee of the other orbit.

The worst relative spacecraft locations occur when the two altitude time histories are identical and in phase. In one bad case, the two orbits are also coplanar. In the other bad case, the two orbits have no along-track separation. These cases are unobservable with a $1/r^2$ gravitational force,[7] but secular J_2 effects make them marginally observable at nonzero inclinations.

Several cases have been run to test out the dependence on separation direction. In case 4 of Table 1, spacecraft B leads spacecraft A by 100 km in exactly the same orbital plane and with its altitude time history identical to that of spacecraft A. Spacecraft A's maximum across-track position standard deviation increases to 234.3 m, up from 0.64 m in case 1. Thus, a lack of across-track separation coupled with a lack of perigee separation leads to a degradation in across-track orbit determination accuracy.

A similar result holds when there is minimal along-track separation and the altitude time histories are identical; see case 5 of Table 1. In this case, spacecraft A's maximum along-track position standard deviation is 287.6 m, as opposed to 1.27 m for case 1. Although secular J_2 effects induce observability in an otherwise unobservable case, a lack of along-track separation coupled with a lack of altitude separation degrades the along-track accuracy.

Case 6 of Table 1 tests what happens when one spacecraft orbits the other. The two spacecraft orbits are coplanar and have the same apogee and perigee altitudes, but their arguments of perigee are 180 deg out of phase. The fact that spacecraft B orbits spacecraft A shows up in the minimum and maximum along-track separation of spacecraft B from spacecraft A. In all other respects this case is similar to the nominal case. According to Markley,[7] this case should be strongly observable. The accuracy of this case is comparable to that of case 1, which confirms that practical observability holds for this situation.

The batch duration affects the accuracy. If it is increased to two orbits while the number of samples remains the same, then the accuracy improves, as shown by case 7 of Table 1. The greatest improvements compared to case 1, those in the along-track and altitude directions, are due largely to a 12-fold decrease in the drag parameter's uncertainty.

The angular accuracy of the $\boldsymbol{r}_{BA}$ measurement, σ_{ang}, has a significant impact on the predicted estimation accuracy. A case has been tried in which σ_{ang} is increased from its 0.2 arcsec nominal value to a value of 2.0 arcsec, which is more typical of what would be available from a high-performance star sensor system. All other orbital and system characteristics have been kept the same as in the nominal case. These results are reported as case 8 in Table 1. They show from 4- to 6-fold position accuracy decreases, which is not bad considering the 10-fold decrease in the angular sensor accuracy.

The effects of orbital parameters have been investigated. For comparison purposes, the following characteristics have been held constant: Spacecraft B leads Spacecraft A by a nearly constant along-track separation of about 100 km. The orbital planes are slightly different so that the maximum across-track separation is about 100 km. The sensor accuracies are $\sigma_{\text{mag}} = 0.1$ m, $\sigma_{\text{ang}} = 0.2$ arcsec, and $\sigma_{\text{dirmin}} = 0.1$ m. The data batch consists of $N = 1501$ samples, and intersample spacing is varied from case to case to keep the batch interval equal to one orbital period.

The effects of altitude, eccentricity, and inclination of the two spacecraft orbits have been investigated. Inclination of the average orbital plane has little or no effect on the system accuracy if the nominal relationship between the two spacecraft orbits is maintained. Table 2 reports the effects of the altitude and eccentricity of the two spacecraft orbits. Case 1 of Table 2 is the same nominal case as case 1 of Table 1. Cases 1, 9, and 10 of Table 2 show a modest degradation of position accuracy with increases in orbital altitude. At geosynchronous altitude, case 10, the positional standard deviations are about six times larger than for LEO. Case 11 of Table 2 gives results for a pair of orbits with significant eccentricity. Its maximum position component standard deviations are only slightly larger than those of a circular LEO.

Orbital inclination has a marked effect on system accuracy in two special cases. These correspond to the two unobservable cases noted by Markley: the cases of identical altitude time histories for the two spacecraft and either zero along-track separation or zero across-track separation.[7] As earlier noted, secular J_2 effects induce observability in these otherwise unobservable cases if the orbit is inclined. At any appreciable inclination J_2 has a strong beneficial effect, as witnessed by cases 4 and 5 of Table 1, which fall into these categories but have inclinations of 45 and 90 deg, respectively. A case similar to case 4, but with 0.25-deg inclination, produces a maximum across-track position standard deviation of 3.7×10^6 m. At zero inclination all such cases revert to being unobservable.

A case has been tried with two spacecraft in very different orbits. Spacecraft A is in a LEO like the nominal case. Spacecraft B is in a 12-h orbit, with an apogee altitude of 20,299 km and a perigee altitude of 20,165 km. In addition, the two spacecraft are in very different orbital planes. Sensor accuracies like those of the nominal case are used. The data batch contains 1501 samples with a sample spacing of 15.32 s. This translates into a data interval that includes four orbits of spacecraft A, but only slightly more than one-half of an orbit of spacecraft B. This case does not consider the data loss that would occur due to occulting of spacecraft B by the Earth.

The results for this case are very good. Spacecraft A's maximum position standard deviations are 0.25 m along track, 0.24 m across track, and 0.01 m in altitude. Spacecraft B's maximum position standard deviations are 0.68 m along track, 0.95 m across track, and 0.02 m in altitude. One might expect these results to be even better based on the large separations between the spacecraft. Unfortunately, the growth in σ_{dir} due to its $\rho_{BA} \cdot \sigma_{\text{ang}}$ dependence probably militates against increased accuracy in this case.

Table 2 Spacecraft A position standard deviations as functions of orbital apogee and perigee

Case	Apogee, km	Perigee, km	Maximum component σ, m A-T	C-T	Altitude
1	585	515	1.27	0.64	0.82
9	1,000	930	1.36	0.68	0.88
10	35,912	35,659	7.72	3.93	5.02
11	3,200	500	1.67	0.73	1.15

Another interesting case is that of two ballistic missiles. It might be possible to use this technique to do midcourse orbit determination for a pair of ballistic missiles during their coast phase. The case that has been considered is that of two ballistic missiles that must travel from a launch site to a target that is 75 deg away on the Earth's surface (8300 km away). The missiles travel in the minimum energy orbit that is required to traverse this distance, an orbit with an apogee altitude of 1289 km. Missile B leads missile A by 85.8 km to 101.6 km of along-track separation, and they have a maximum across-track separation of 101.6 km. The data batch interval begins when missile A leaves the sensible atmosphere, at 100 km altitude, and the interval ends when missile B starts to re-enter the atmosphere, at 100 km of altitude. For a sample interval of 1.00 s this translates into a total of $N = 1665$ samples.

The results for this case are reasonably good. The maximum along-track standard deviation is 27.79 m, the maximum across-track standard deviation is 15.47 m, and the maximum altitude standard deviation is 12.20 m. The main reason why these results are not as good as comparable LEO cases is the shortness of the batch interval. It is just 1664 s long. The other LEO cases are 5745 s long, the length of a full orbit.

V. Additional Results and Discussion

The purpose of this section is briefly to discuss results obtained by filtering simulated truth-model data and to discuss some operational practicalities of the proposed system. The truth-model results serve to study whether nonlinear effects are important and to check the correctness of the covariance analysis. The operational issues address some computational, sensor, and modeling requirements for the system.

Truth-model data has been generated, and this data has been filtered using the batch filter of Sec. III. The truth model that has been used is simplistic. It uses the dynamic and measurement models of Sec. III. It inputs a truth value of $\boldsymbol{p}$ into these models and uses a random number generator to generate the measurement noise sequences $n_{\rho(k)}$, $n_{2(k)}$, and $n_{3(k)}$.

A limited number of truth-model data batches have been run through the filter. Not enough runs have been done for a meaningful Monte Carlo statistical analysis, but these limited results serve to confirm the covariance analyses results. For example, none of the truth-model maximum position component errors has exceeded the corresponding maximum position component standard deviation by more than a factor of three. This confirms that the 3-σ rule can be applied to the maximum component standard deviations of Sec. IV to predict the worst-case performance on actual data. These results also demonstrate that nonlinearities do not significantly affect performance for the levels of sensor accuracy considered in this study.

The filter converged rapidly for fairly good initial guesses of the orbital parameters. For the LEO cases that have been considered, the maximum initial position errors ranged from 70 to 560 km. For the higher altitude orbits, the maximum initial position errors ranged as high as 4400 km. The filter took between 3 and 98 Gauss–Newton iterations to converge for all cases considered. Many cases converged in under 15 iterations. Convergence can take a long time if the initial guess is poor or if the Gauss–Newton step-length restriction is too conservative. If Eq. (10) is used to define $\rho_{BA\,\text{mod}(k)}(\boldsymbol{p})$, then the filter requires many more iterations to converge from a poor initial guess.

The convergence and accuracy of a typical case are shown by the data in Table 3. This case corresponds to actual orbits and sensor accuracies as in the nominal case, which is reported as case 1 of Table 1. The filter started with an initial guess whose maximum

Table 3 Typical spacecraft A results for filtering of truth-model data

Element set	M_{0A}, rad	M_{1A}, rad/herg	M_{2A}, rad/herg^2	e_A	ω_{0A}, rad	λ_{0A}, rad	i_A, rad
First guess	3.1988325	0.88401598	1.5978×10^{-7}	0.00545186	1.4702654	4.8763801	0.8105309
Filter output	3.1736923	0.88331611	1.3782×10^{-7}	0.00505183	1.4451398	4.8386810	0.7853982
Truth model	3.1736997	0.88331598	1.5378×10^{-7}	0.00505186	1.4451326	4.8386810	0.7853982

spacecraft A position errors were 562 km along track, 256 km across track, and 32 km in altitude. It converged in nine Gauss–Newton iterations. Table 3 shows three sets of orbital elements for spacecraft A: the filter's initial guesses, the filter's solutions, and the truth values. Except for M_{2A}, the filter outputs are very close to the truth-model values, and they are orders of magnitude closer than are the initial guesses. (The time unit "herg" that is used in Table 3 is equal to 806.81359 sec.)

Memory and execution time requirements are not large by current standards. Typical run time in Fortran on a 100-MHz Pentium processor is 2.6 s per iteration for a case with 1501 samples. The run time varies linearly with the number of samples in the data batch. The executable code uses double precision arithmetic and occupies 177 kbytes of memory, which includes space for data storage.

Several practical aspects of the proposed system will need to be considered in the future. One such aspect is the issue of field-of-view requirements for the instrument that detects the direction of spacecraft B in spacecraft A's coordinate system. The best spacecraft orbital relationships involve either significant across-track deviations or one spacecraft orbiting the other. If the direction telescope had a narrow field of view, then spacecraft A would have to be slewed to keep spacecraft B in the sensor's field of view. Alternatively, Spacecraft B's position might be sampled only as often as it entered the direction telescope's field of view.

Most of the cases considered in this paper assume that the two spacecraft stay relatively near each other. This might be necessary to allow the sensing instrumentation on spacecraft A to detect spacecraft B. Given a maximum separation limit, it might be necessary to make frequent adjustments to one of the spacecraft's orbits to maintain the proper separation.

The issue of possible biases and drift in the sensors is an important one. If the system is to succeed, it will need a way to use extra data to determine biases during a calibration period. Subsequent accuracy will depend heavily on having low sensor drift rates. Therefore, future work must consider the question of what type of sensor performance is needed and whether it can be achieved.

The impact of orbit propagation inaccuracy has been largely ignored in the present study. Orbit propagation inaccuracy may be the major limiting factor to a real system's performance. Therefore, this issue must eventually be addressed. It may be possible that the best filter for this system would be one that estimated several configuration parameters, such as a drag parameter and a solar radiation pressure parameter for each spacecraft, in addition to the orbit elements.

This is a proof-of-concept study of the proposed system. It is likely to be optimistic in its results due to factors that have been neglected. These results represent a best-case scenario that will be achieved in practice only if the practicalities mentioned earlier do not turn out to be the main limits to performance.

VI. Conclusions

This paper has proposed and analyzed a novel system for autonomously determining the orbits of a pair of Earth-orbiting spacecraft. The system makes use of measurements of the position vector of one of the spacecraft relative to the other in an inertially oriented reference system. The system filters these measurements using physically based orbital dynamics models. The system does not need exact a priori knowledge of either spacecraft's orbit.

This system is absolutely observable in all but a few special cases that occur at zero inclination. The estimation accuracy depends strongly on the relative spacecraft positions. Accuracy decreases as the spacecraft get too near to each other. Accuracy also decreases if the two spacecraft have the same altitude time history and there is either too little along-track separation between the spacecraft or too little separation between their orbital planes.

The covariance of a 1-orbit filtering run has been computed for a representative case, one with measurement accuracies of 0.1 m in relative range and 0.2 arcsec in relative direction and with the two spacecraft in similar LEO with 100-km along-track and across-track separations. This case has a predicted position accuracy of better than 1.3-m rms per axis.

Acknowledgment

Patrick Binning, one of the reviewers of this paper, was responsible for pointing out the connection between this work and that of Landis Markley.

References

[1]Tapley, B. D., Ries, J. C., Davis, G. W., Eanes, R. J., Schutz, B. E., Shum, C. K., Watkins, M. M., Marshall, J. A., Nerem, R. S., Putney, B. H., Klosko, S. M., Luthcke, S. B., Pavlis, D., Williamson, R. G., and Zelensky, N. P., "Precision Orbit Determination for TOPEX/POSEIDON," *Journal of Geophysical Research*, Vol. 99, No. C12, 1994, pp. 24,383–24,404.

[2]Wu, S. C., Yunck, T. P., and Thornton, C. L., "Reduced-Dynamic Technique for Precise Orbit Determination of Low Earth Satellites," *Journal of Guidance, Control, and Dynamics*, Vol. 14, No. 1, 1991, pp. 24–30.

[3]Hoech, R., Bartholomew, R., Moen, V., and Grigg, K., "Design, Capabilities and Performance of a Miniaturized Airborne GPS Receiver for Space Applications," *Proceedings of the IEEE Position, Location, and Navigation Symposium* (Las Vegas, NV), Inst. of Electrical and Electronics Engineers, New York, 1994, pp. 1–7.

[4]Chory, M. A., Hoffman, D. P., Major, C. S., and Spector, V. A., "Autonomous Navigation—Where We Are in 1984," *Proceedings of the AIAA Guidance and Control Conference* (Seattle, WA), AIAA, Washington, DC, 1984, pp. 27–37 (AIAA Paper 84-1826, Aug. 1984).

[5]Chory, M. A., Hoffman, D. P., and LeMay, J. L., "Satellite Autonomous Navigation—Status and History," *Proceedings of the IEEE Position, Location, and Navigation Symposium* (Las Vegas, NV), Inst. of Electrical and Electronics Engineers, New York, 1986, pp. 110–121.

[6]Psiaki, M. L., Huang, L., and Fox, S. M., "Ground Tests of Magnetometer-Based Autonomous Navigation (MAGNAV) for Low-Earth-Orbiting Spacecraft," *Journal of Guidance, Control, and Dynamics*, Vol. 16, No. 1, 1993, pp. 206–214.

[7]Markley, F. L., "Autonomous Navigation Using Landmark and Intersatellite Data," AIAA/American Astronautical Society Astrodynamics Conf., Seattle, WA, Aug. 20–22, 1984 (AIAA Paper 84-1987, Aug. 1984).

[8]Blackmon, J. B., and Stone K. W., "Digital Image System for Determining Relative Position and Motion of In-Flight Vehicles," U.S. Patent 5,493,392, Feb. 1996.

[9]Ananda, M. P., Bernstein, H., Cunningham, K. E., Feess, W. A., and Stroud, E. G., "Global Positioning System (GPS) Autonomous Navigation," *Proceedings of the IEEE Position, Location, and Navigation Symposium*, Inst. of Electrical and Electronics Engineers, New York, 1990, pp. 497–508.

[10]Menn, M., "Autonomous Navigation for GPS via Crosslink Ranging," *Proceedings of the IEEE Position, Location, and Navigation Symposium* (Las Vegas, NV), Inst. of Electrical and Electronics Engineers, New York, 1986, pp. 143–146.

[11]Herklotz, R. L., "Incorporation of Cross-Link Range Measurements in the Orbit Determination Process to Increase Satellite Constellation Autonomy," Ph.D. Thesis, Dept. of Aeronautics and Astronautics, Massachusetts Inst. of Technology, Cambridge, MA, Dec. 1987.

[12]LeMay, J. L., Brogan, W. L., and Seal, C. E., "High Altitude Navigation Study (HANS)," The Aerospace Corp., Rept. TR-0073(3491)-1, El Segundo, CA, June 1973; also, Defense Technical Information Center Rept. AD-773 835, June 1973.

[13]Roberson, R. E., "Gravity Gradient Determination of the Vertical," *American Rocket Society Journal*, Vol. 31, No. 11, 1961, pp. 1509–1515.

[14]Metzger, E. H., Jircitano, A., and Affleck, C., "Final Report: Satellite Borne Gravity Gradiometer Study," Bell Aerospace Textron, Rept. 6413-950001, Buffalo, NY, March 1976.

[15]Psiaki, M. L., "Autonomous Orbit and Magnetic Field Determination Using Magnetometer and Star Sensor Data," *Journal of Guidance, Control, and Dynamics*, Vol. 18, No. 3, 1995, pp. 584–592.

[16]Gill, P. E., Murray, W., and Wright, M. H., *Practical Optimization*, Academic, New York, 1981, pp. 133–140.